NASA Technical Memorandum 100134

Performance and Combustion Characteristics of Direct-Injection Stratified-Charge Rotary Engines

Hung Lee Nguyen
Lewis Research Center
Cleveland, Ohio

December 1987

NASA

PERFORMANCE AND COMBUSTION CHARACTERISTICS OF DIRECT-INJECTION STRATIFIED-CHARGE ROTARY ENGINES

Hung Lee Nguyen
National Aeronautics and Space Administration
Lewis Research Center
Cleveland, Ohio 44135

SUMMARY

Computer simulations of the direct-injection stratified-charge (DISC) Wankel engine are used to calculate heat release rates and performance and efficiency characteristics of the Deere model 1007R engine test rig. Engine pressure data are used in a heat release analysis to study the effects of heat transfer, leakage, and crevice flows. Predicted engine performance data are compared with experimental test data over a range of engine speeds and loads. An examination of methods to improve the performance of the Wankel engine with advanced spark timing, reduced leakage, higher compression ratio, and turbocharging is also presented.

INTRODUCTION

The direct-injection stratified-charge (DISC) Wankel engine is currently being evaluated by NASA as a future advanced powerplant for light commercial aircraft and similar applications (ref. 1). The DISC Wankel engine offers attractive advantages over reciprocating engines. These advantages include higher airflow capacity, higher power-to-weight ratio, simpler and more compact shape, fewer moving parts, lower noise levels, and less vibration. The DISC combustion concept is insensitive to fuel cetane and octane ratings. With it, the Wankel engine can be designed for operation with jet-fuel, diesel, or multi-fuel capability (refs. 1 and 2).

Despite its apparent advantages, the Wankel engine has achieved only limited acceptance to date. Its allegedly poorer cycle efficiency than that of a comparable piston engine may be a deterrent to the mentioned applications. Although published data are scarce, an indicated-thermal-efficiency shortfall of about 5 percentage points (e.g., 28 percent as opposed to 33 percent for a comparable piston engine) is thought to be representative at this time. In the past, research to clarify and resolve this issue was impeded by the lack of both appropriate engine-simulation computer models and an adequate engine test rig. This paper reports the first coordinated use of recently developed computer models and a new, high-performance test rig to study the effects of combustion rate phenomena and various loss mechanisms in a DISC Wankel engine.

The objective of this investigation is twofold. First, the combustion rate and performance loss mechanisms of the Deere model 1007R Wankel engine test rig were analyzed. Experimental pressure data obtained from the 1007R engine rig were used with the Massachusetts Institute of Technology (M.I.T.) heat release computer model to evaluate the fuel burning rate and loss mechanisms (such as heat transfer to structures, crevice volumes, and gas leakage). Second, the M.I.T. engine-simulation model was used to predict the performance

of the 1007R engine rig. The predictions were then compared with experimental data. The engine simulation models were also used to examine how DISC Wankel engine performance varies with changes in engine design and operating conditions. Potential performance improvements of the DISC Wankel engine with advanced spark timing, reduced leakage, higher compression ratio, and turbocharging were investigated.

MODELS DESCRIPTION

Two thermodynamic simulation models were used to predict the performance of DISC Wankel rotary engines. These models were developed by researchers at Sloan Automotive Laboratory, Massachusetts Institute of Technology (ref. 3), under a NASA grant. The first type of computer model may be used to determine the combustion heat release rate from measured chamber pressure by using a heat release analysis based on a first-law thermodynamic analysis on the contents of the engine combustion chamber. The combustion chamber is treated as an open thermodynamic system, and its contents are effectively modeled as uniform and homogeneous. Thermodynamic properties of the chamber contents are represented by a simple linear function of temperature for the ratio of specific heats γ (ref. 4). The fuel chemical energy released inside the combustion chamber is accounted for by all the major energy and mass transport mechanisms (heat transfer, leakage, and crevice volume effects) in addition to the net thermal efficiency and the sensible internal energy changes of the fuel charge. In performing the heat transfer calculation, the convective heat transfer to combustion chamber walls is calculated in addition to the heat transfers associated with flow into and out of crevices. Heat transfer due to flows through leakage paths is also simulated. The forced convective heat transfer is based on the form proposed by Woschni (ref. 5). The heat transfer coefficient appearing in the Woschni equation takes the following form:

$$h = 131.0\, R^{-0.2}\, p^{0.8}\, T^{-0.53}\, w^{0.8} \tag{1}$$

where R is the rotor radius, P is the chamber pressure, T is the chamber average temperature, and w is the characteristic speed given by

$$w = 2.28\, C_1\, U_R + 0.324\, C_2 \left(\frac{V_{disp}}{V_{IPC}}\right)\left(\frac{P_f - P_m}{P_{IPC}}\right) T_{IPC} \tag{2}$$

where U_R is the mean rotor speed, V is the chamber volume, the subscript IPC refers to conditions at intake port closing, P_f and P_m are firing and motoring pressures, respectively, and V_{disp} is the displacement volume. The symbols C_1 and C_2 are scaling coefficients and are adjusted according to the calibration procedure described in the following section. Crevice and leakage phenomena are combined; that is, the leakage flow path to an adjacent chamber is assumed to occur by way of a crevice region.

To assist in formulating the combustion model, a single universal empirical model which defines the rate of heat release for a range of speeds and loads was used (ref. 3). From the start of combustion at crankshaft angle θ_s, the heat release rate rises linearly to $(dQ/d\theta)_m$, the peak rate of heat release, which occurs at θ_m, the crankshaft angle position at peak rate of heat release. The heat release rate then decays exponentially with a time constant τ, until the exhaust port begins to open. An integral constraint

defines the sum of the integrated heat release rates between the intervals θ_s to θ_m, and θ_m to exhaust port opening, as the combustion efficiency n_{comb} multiplied by the energy of the injected fuel. This integral constraint was used to aid in computing the four parameters appearing in the heat release empirical model. Therefore, only three of the four model parameters need to be specified, with the fourth being determined by the constraint. From θ_s to θ_m, the rate of heat release is given by

$$\frac{dQ}{d\theta} = \frac{dQ}{d\theta_m}\left[\frac{(\theta - \theta_s)}{(\theta_m - \theta_s)}\right] \tag{3}$$

For a crankshaft angle greater than the peak rate location θ_m, the rate of heat release is given by

$$\frac{dQ}{d\theta} = \frac{dQ}{d\theta_m} \exp\left[\frac{(\theta - \theta_s)}{\tau}\right] \tag{4}$$

with τ as the fourth value given by the integral constraint

$$\tau = \left[\frac{n_{comb}}{\frac{dQ}{d\theta_m}} - \frac{1}{2}(\theta_m - \theta_s)\right] \tag{5}$$

This heat release model can provide both a useful check on the quality of measured chamber pressure data, and an accurate method for predicting combustion rates from measured chamber pressure data.

The second numerical simulation model has been used to predict the development of the chamber pressure with time, and thereby the engine performance, from a prespecified combustion rate. The engine simulation model divides the complete engine cycle into the following periods: intake, compression, combustion (and expansion), and exhaust. The engine simulation is based on a first-law thermodynamics analysis of the engine combustion chamber with the following major assumptions:

(1) Quasi-steady, one-dimensional compressible flow equations are used to calculate the mass flows through the ports.

(2) The intake and exhaust manifolds are treated as infinite plenums with specified pressure and temperature histories.

(3) A one-zone combustion model in which the combustion rate is specified by a heat release rate equation is used. This one-zone model describes the chamber contents by a time-varying average overall equivalence ratio and temperature.

(4) Heat transfer to rotor and housings is modeled as turbulent convection over a flat plate where the corresponding Nusselt-Reynolds number correlation is used. Also, heat transfer to crevice walls is based on crevice gas properties evaluated at the crevice wall temperature. Radiative heat transfer is neglected.

(5) Crevices are modeled as containing gas at chamber pressure and wall temperature.

(6) Leakage occurs from a crevice region to an adjacent chamber (at lower pressure). One-dimensional, quasi-steady compressible flow equations are used to model leakage flows.

(7) Thermodynamic properties (enthalpy and density) of the chamber contents are specified as functions of chamber temperature, pressure, and average equivalence ratio. The ideal gas law is obeyed throughout the cycle.

The heat release rate and the engine simulation programs can be used as diagnostic tools to predict the performance of DISC Wankel engines when changes in the engine design and operating conditions are made.

MODELS CALIBRATION AND VALIDATION METHODOLOGIES

The calibration and validation strategies of the heat release and engine simulation programs are discussed next. The heat release program and the engine cycle simulation involve a number of submodels containing empirical constants which require calibration against experimental data. For example, the following values of empirical constants in various submodels must be specified: the two scaling factors in the heat transfer model, the values for the crevice volume and the leakage area, the wall temperature, the ratio of specific heats, and the values of the discharge coefficients. Experimental data obtained from the firing 1007R engine rig were used in the following calibration and validation procedures:

(1) Experimental ensemble-averaged pressure traces versus crank angle data were used as input to the heat release program. As a starting point, estimates for the values of the heat transfer constants, crevice volume, leakage area, and discharge coefficients were used. Computations of the individual heat release rates and the integrated heat release (gross heat release) rates were performed. The gross heat release should be zero before start of combustion. At the end of combustion, the curve should be nearly flat, with a value very close to the fuel energy (mass of fuel multiplied by its lower heating value per unit mass). Therefore, the gross heat release curves provide useful checks for the heat release model.

(2) From the individual heat release rates computed at varying speed and load points, an average heat release rate was calculated.

(3) The empirical heat release rate model was then fitted to the average calculated heat release rate. A set of four best-fitted parameters (θ_s, $(dQ/d\theta)_m$, θ_m, and τ) was obtained.

(4) The heat release rate obtained in the preceding step was used as input to the engine simulation program. The predicted pressure traces were then compared with experimental ensemble-averaged pressure traces. This iteration scheme was repeated until convergence between the computed and experimental ensemble-averaged pressure traces was obtained. This study was the baseline case where all the heat loss mechanisms were considered.

HEAT RELEASE PARAMETRIC ANALYSIS

In order to investigate the effects of heat transfer, crevice volume, and leakage area on heat release and engine performance, the following parametric study was performed.

(1) The fitted heat release rate from the baseline case was used as input to the engine simulation. Heat transfer was neglected. A corresponding pressure versus crank angle curve was obtained.

(2) The pressure data obtained in the previous step was used to calculate the corresponding heat release rate profile. This heat release rate profile was used in the fitting procedure to obtain four new best-fitted parameters in the empirical heat release rate model. This heat release rate model was then used in the engine simulation to compute a new pressure trace versus crank angle. This new pressure trace was used as input to the heat release rate program to calculate the new heat release rate profile. This iteration scheme was repeated until consistency was achieved.

DESCRIPTION OF ENGINE

The baseline Wankel engine selected for the present study is the single rotor, stratified-charge research rig engine, which was designed by the Rotary Engine Division of John Deere Technologies International, Inc., under a NASA contract. Model designation for this engine is 1007R, where the first digit indicates a single rotor and the last digits indicate the total engine displacement to the nearest deciliter. The 1007R engine was designed, fabricated, and tested by John Deere in 1984 to 1986 as a rig engine for high-output, aircraft duty cycle conditions.

Table I presents the geometric data for the 1007R baseline Wankel engine. This stratified-charge rotary engine uses two fuel injectors per rotor. The arrangement of the injector and igniter in the rotor housing is shown in figure 1. The igniter provides the start of combustion for the pilot spray. The pilot spray, once ignited, provides the ignition source for the fuel from the main injection nozzle. The main nozzle has multiple holes to allow efficient utilization of the combustion chamber volume at high loads. The engine was turbocharged and intercooled to increase specific output and to improve fuel consumption. Peripheral intake and exhaust ports were used. The fuel used for this series of tests was Jet A.

Pressure in the combustion chamber was measured by a series of four pressure transducers placed around the rotor housing. The locations of the transducers are arranged such that the signals from two adjacent transducers overlap during part of the cycle. Figure 2 shows the position of the pressure transducers in the engine rotor housing. The minimum overlap of 22 shaft degrees exists between the third and fourth transducer locations. Because of limitations in the placement of the transducers, measurements during combustion are split between the first and second transducers. The first transducer measures combustion pressure until 40° after-top-center (ATC); the second transducer begins measuring combustion pressure at 9° ATC.

A 720-pulse-per-revolution shaft encoder was driven from the engine output shaft at one-third speed. The encoder was used to provide a cycle trigger and

sample signals at 1.5 crankshaft-degree intervals. A four-channel, digital oscilloscope capable of ensemble averaging the pressure signals over a specified number of cycles was used to capture, average, and splice the output from the four transducers. The pressure data used in this analysis were ensemble averaged over 50 engine cycles.

RESULTS AND DISCUSSION

Results of Heat Release Analysis

Figure 3 shows the results for the combustion heat release rates at brake mean effective pressures (BMEP's) ranging from 298 to 890 kPa at an engine speed of 4000 rpm. The rate of combustion heat release was plotted as a function of crankshaft angle. Each curve was calculated by using an ensemble average of 50 consecutive cycles of the experimental pressure data. The general trend of these figures shows an increase in the value of the peak rate, hence an increase in combustion efficiency, as BMEP is increased. The double peak in the heat release rate at 693 kPa BMEP indicates that the accuracies of the heat release analysis rely on the accuracies of the experimental pressure data. The heat release analysis uses the derivative of the chamber pressure, hence smooth and highly resolved pressure data are necessary to obtain accurate heat release rate results. Experimental pressure data analyzed with the heat release rate program should also be ensemble averaged over a large number of carefully measured, single-cycle pressure data so that the effects of cycle-to-cycle variations are not overly weighted (ref. 6). The double peak in the heat release rate may have resulted from the effects of cycle-to-cycle variations due to ensemble averaging of only 50 cycles of pressure data.

All the heat release rate curves exhibit three stages of combustion. The first stage of combustion starts at approximately 25° before-top-center (BTC). The second stage of combustion starts at about 5° BTC and ends at approximately 40° ATC. The third stage of combustion starts at the end of the second stage and proceeds well into the expansion stroke. It should be noted that the heat release rate results during the second stage are sensitive to the inaccuracies in the pressure data. As BMEP decreases, the distinction between the second and third stage of combustion becomes less clear.

A complete understanding of the combustion process would require detailed modeling of the compressible viscous air motion, fuel spray penetration, droplet breakup and evaporation, air entrainment into the spray, turbulent diffusion, combustion kinetics, and so on. The observed early burning stage of combustion is evident by the result of pilot spray combustion and is denoted as the pilot stage. Its occurrence agrees with the injection timing of the pilot spray (see table II). The description of diesel combustion by Watson et al. (ref. 7) may be used here to explain the following two stages of combustion observed in the 1007R rig engine. Watson et al. proposed that the apparent fuel burning rate in diesel engines could be expressed as the sum of two components, one relating to premixed burning and the other to diffusion-controlled burning. In the premixed stage, combustion of the fuel which has already mixed with air to within the flammability limits occurs fairly rapidly. Once the premixed fuel and air mixture has been consumed, combustion in the next stage is controlled by the lower rate, at which the fuel-air mixture becomes available for diffusion burning. This stage of combustion continues

well into the expansion stroke and asymptotically approaches zero. The integrated heat release rates at four typical loads are presented in figure 4. The integrated heat release rates indicate that approximately 5 percent of the fuel burns during the pilot stage, little more than half of the fuel burns in the premixed stage, and the majority of the remaining fuel burns in the diffusion stage. The integrated heat release rates also indicate that the amount of fuel burned before top-dead-center increases as load decreases. Figure 4 also shows performance loss mechanisms. The lowest curve is the net heat release; it represents the net thermal efficiency and the sensible internal energy changes of the charge. The next curve shows the effect of adding heat transfer to engine structures. The highest curve shows the gross heat release, which combines the effects of adding heat transfer, crevice volume, and leakage area. This is the computed gross heat release curve, which represents the amount of chemical energy released as thermal energy by combustion. The straight line along the top of each part of figure 4 represents the fuel chemical energy within the chamber; that is, the mass of fuel in the chamber multiplied by the lower heating value per unit mass. The breakdown of these loss mechanisms at all four loads for the 1007 rig engine is given in table III.

Figure 5 shows the comparison of computed and experimental pressure profiles at four loads at 4000 rpm. The peak pressure in the simulation is overpredicted. The pressure values in the simulation are underpredicted during compression; this suggests that the port area, or discharge coefficient, is not correct in the model. In addition, the DISC Wankel simulation assumes that fuel is injected at the rate at which it is burned, as defined by a prespecified heat release equation.

To complete the formulation of the combustion model, a single, universal heat release rate curve (fig. 6) is generated by averaging the rates shown in figure 3. As a first attempt, the empirical heat release rate model described in the section Models Description was used to represent the rate of heat release in the numerical simulation. The empirical heat release rate was fitted to the average heat release rate curve, and the results of the model parameter values are

$$\theta_s = 15.24^\circ \text{ BTC}$$

$$\theta_m = 20.55^\circ \text{ ATC}$$

$$(dQ/d\theta)_m = 0.029 \text{ (1/deg)}$$

$$\tau = 16.24^\circ$$

The calibration of the submodels of heat release, heat transfer, leakage, crevice effects, and others resulted in additional parameter values in the 1007R rig engine simulation as follows:

Heat transfer constants	
C_1	0.4
C_2	0.5
Leakage area per apex, cm^2	0.01
Crevice volume, cm^3	0.573
Discharge coefficients	
Intake	0.8
Exhaust	0.7

Estimated temperatures of the rotor face and measured temperatures of the side and rotor housing surfaces at various operating conditions were used in the simulation. The effects of various operational parameters on the performance of the 1007R rig engine and its predicted results are discussed next.

Engine Performance Results

Calculations were carried out for the 1007R turbocharged rig engine at 4000 rpm at four loads. The simulation output was checked against performance test data. The various calculated parameters (i.e., volumetric efficiency, power output, indicated specific fuel consumption (ISFC), and exhaust temperature) are compared with experimental results in figures 7 and 8. Only indicated quantities were computed, since friction was not included in the simulation model.

Figure 7 shows the comparison of the indicated values of the power output and specific fuel consumption predicted by the simulation and experimental values of brake horsepower (BHP) and brake specific fuel consumption (BSFC), respectively, at 4000 rpm at four loads. There is good agreement in the trend of indicated power output predicted from the simulation and brake horsepower from engine test data. The brake horsepower values are about 28 percent lower than indicated horsepower values predicted from simulation. The predicted indicated specific fuel consumption values are about 26 percent lower than the measured brake specific fuel consumption.

Figure 8 shows the comparison of the volumetric efficiency and exhaust temperature values predicted by the simulation with the engine data. Comparison of the values for volumetric efficiency shows differences varying from 2 to 22 percent. The simulation model overpredicted the exhaust temperature by 16 to 44 percent. The values of predicted performance data are listed in table IV.

Figure 9 presents the 1007R turbocharged engine performance map predicted by the simulation model. Predicted engine performance and ISFC data are presented.

The effects of changes in equivalence ratio, spark timing, compression ratio, turbocharging, and leakage area on performance characteristics of the 1007R rig engine were studied by the simulation model, and the results are discussed next. Tests were carried out for the following reference condition: 4000 rpm, 890 kPa BMEP. To make these parametric studies, one parameter was changed at a time while the other parameters were kept at the reference condition.

The effect of equivalence ratio. - Variation in power output, ISFC, and exhaust temperature with equivalence ratio is shown in figure 10.

The effect of advanced spark timing. - Figure 11 shows the effect of advanced spark timing on the mass burned fraction, chamber pressure and temperature, and power output of the 1007R rig engine at 4000 rpm, equivalence ratio ϕ = 0.65, and 890 kPa BMEP. The value of the spark timing was varied from 20° to 8° BTC. The normalized mass fraction burned at three different spark timings (20°, 15°, and 8° BTC) indicates that the fuel is burned faster and

earlier in the cycle with early spark timing. The simulation also predicts significant increase in the peak pressure with early spark timing. The chamber temperature near top-dead-center (TDC) and the total work output per cycle from the pressure-volume diagrams shown in figure 11 also increase with early spark timing.

Figure 12 shows the effect of advanced spark timing on the power output, indicated mean effective pressure (IMEP), ISFC, and exhaust temperature for the 1007R rig engine (4000 rpm, 890 kPa BMEP). The model predicts an increase in power output and IMEP with early spark timing. The model also predicts a decrease in ISFC and exhaust temperature with early spark timing.

The effect of combustion rate. - Understanding the combustion process plays an important role in the optimization of engine performance and efficiency of the Wankel engine. To change the combustion rate in the simulation of the 1007R engine test rig, the combustion duration was adjusted. The combustion duration is defined as the crankshaft angle interval from 10 percent mass fraction burned to 90 percent mass fraction burned. The crankshaft angle interval between the actual spark timing and 10 percent mass fraction burned defines the ignition delay period. A change in the combustion duration was induced by a change in the values of θ_m (the crankshaft angle position at peak rate of heat release), the values of θ_s (the spark timing), and the values of $(dQ/d\theta)_m$ (the peak rate of heat release). The values of the area under the rate of heat release curve, $(dQ/d\theta)$ of equation (3), remained constant (i.e., the amount of fuel burned was the same for all the cases studied). The time constant τ of equation (4) was calculated by using equation (5). Figure 13 shows the five combustion heat release rates with combustion duration ranging from 15.5° to 114.2° crankshaft angle interval.

Figure 14 presents the effect of combustion duration on the power output, thermal efficiency, ISFC, and exhaust temperature for the 1007R rig engine (4000 rpm; 890 kPa BMEP)). The maximum power output was 70.78 hp at 44.4° crankshaft angle burn duration. A minimum ISFC of 0.3896 lb/hp-hr and a maximum IMEP of 1491 kPa were also obtained at this burn duration. The exhaust temperature increased linearly with burn duration for the range of crankshaft angles studied here. Table V summarizes the effect of burn duration on the performance of the 1007R rig engine.

The effect of leakage area. - Leakage past the apex and side seals is an important source of performance loss in the Wankel rotary engine. Eberle and Klomp (ref. 8) predicted that a reduction in leakage area of 5 percent at 2000 rpm will reduce ISFC by 6.5 percent. The side-seal spring modification made by Yamamoto and Mukori (ref. 9) reduces brake specific fuel consumption by 3.5 percent at 1500 rpm over a load range of 1.5 to 4 kg/cm^2 BMEP.

The model used in this study combines apex and side-seal leakage into three side-seal leakage areas. Figure 15 shows the effect of reduced leakage area on power output, IMEP, and ISFC for the 1007R turbocharged rig engine (4000 rpm, 890 kPa BMEP). The model predicts a significant improvement in engine performance with reduced leakage. As the leakage area is reduced from 0.02 to 0 cm^2 per apex, the following improvements are observed: power output is increased by 12.4 percent, IMEP is increased by 12.8 percent, and ISFC is decreased by 15.7 percent. Although a complete elimination of leakage (i.e., zero leakage area) may not be practically possible, even modest reductions in leakage will result in significant performance improvements.

The effect of turbocharging. - Figure 16 shows the effect of turbocharging the 1007R rig engine at 4000 rpm through the intake and exhaust manifold pressures. These results indicate a significant improvement in performance over the naturally aspirated engine. An increase in power output of 32 percent is observed as the intake pressure is increased by 21 percent. An increase in the intake pressure by the same amount also increases the exhaust temperature by 16.8 percent, ISFC by 3.8 percent, and the indicated mean effective pressure (IMEP) by 33 percent.

The effect of higher compression ratio. - The effect of higher compression ratio on the Wankel engine performance was also studied by the simulation model. The compression ratios studied were 7.5 and 8.92. Figure 17 shows the effect of increasing compression ratio on the 1007R rig engine performance (4000 rpm, 890 kPa BMEP). An increase in compression ratio by 16 percent increases the power output by 4 percent. The exhaust temperature and the IMEP also increase with an increase in compression ratio.

The Wankel engine simulation model predicted an improvement in performance with higher compression ratio, turbocharging, and reduced leakage. The predicted performance improvement in the DISC Wankel engine with these concepts is summarized in tables V and VI.

CONCLUSIONS

Computer models of heat release rate and engine simulation of the DISC Wankel engine simulation have been used to study engine performance loss mechanisms and to investigate how the performance of the DISC Wankel engine varies with changes in engine design and operating conditions. Comparison of calculation results with experimental data was provided. The major conclusions which have been drawn from this study are the following:

1. Combustion in the 1007R rig engine displays three distinct stages. The early burning stage 1 of combustion which starts at approximately 25° BTC may be the result of pilot spray combustion. Stage 2 of combustion starts at about 5° BTC and ends at approximately 40° ATC. The third stage of combustion starts at the end of the second stage and proceeds well into the expansion stroke. Stage 2 can be described as a rapidly occurring premixed combustion period, and stage 3 can be described as a slow diffusion-controlled combustion period.

2. The heat release rate profiles indicate an increase in combustion efficiency as BMEP is increased. As BMEP is decreased, the distinction between the second stage and the third stage of combustion becomes less clear.

3. Carefully measured pressure data that are ensemble averaged over a large number of cycles are required to obtain accurate heat release analysis.

4. The crevice volume and leakage area of the 1007R rig engine are small.

5. The engine simulation model predicts significant improvements in the performance of the 1007R rig engine with reduced leakage, higher compression ratio, and turbocharging.

REFERENCES

1. Willis, E.A.; and Wintucky, W.T.: An Overview of NASA Intermittent Combustion Engine Research. AIAA Paper 84-1393, June 1984. (NASA TM-83668.)

2. Mount, R.E.; Parente, A.E.; and Hady, W.F.: Stratified-Charge Rotary Engine for General Aviation. ASME Paper 86-GT-181, June 1986.

3. Roberts, J.A., et al.: Computer Models for Evaluating Premixed and Disc Wankel Engine Performance. SAE Paper 860613, Feb. 1986.

4. Gatowski, J.A., et al.: Heat Release Analysis of Engine Pressure Data. SAE Paper 841359, 1984.

5. Woschni, G.: Universally Applicable Equation for Instantaneous Heat Transfer Coefficient in the Internal Combustion Engine. SAE Paper 670931, 1967.

6. Schock, H.J.; Rice, W.J.; and Meng, P.R.: Experimental Analysis of IMEP in a Rotary Combustion Engine. SAE Paper 810150, Feb. 1981. (NASA TM-81662.)

7. Watson, N.; Pilley, A.D.; and Marzouk, M.: A Combustion Correlation for Diesel Engine Simulation. Diesel Combustion and Emissions, SAE P-86, SAE, 1980, pp. 51-64. (SAE Paper 800029.)

8. Eberle, M.K.; and Klomp, E.D.: An Evaluation of the Potential Performance Gain from Leakage Reduction in Rotary Engines. SAE Paper 730117, 1973.

9. Yamamoto, K.; and Muroki, T.: Development on Exhaust Emissions and Fuel Economy of the Rotary Engine at Toyo Kogyo. SAE Paper 780417, Feb. 1978.

TABLE I. - ENGINE GEOMETRIES

Displacement, in.^{3} (cm^3)	40.424 (662.427)
Eccentricity, in. (mm)	0.607 (15.418)
Generating radius, in. (mm)	4.189 (106.401)
Width of rotor housing, in. (mm)	3.036 (77.114)
Intake port	Peripheral
Port timings, deg ATDC	
Exhaust port opens	209
Exhaust port closes	611
Intake port opens	453
Intake port closes	850
Fuel	Jet A
Lower heating value (LHV), Btu/lb	19 719

TABLE II. - TEST DATA FOR THE 1007R TURBOCHARGED STRATIFIED-CHARGE WANKEL ENGINE

	Case number			
	1	2	3	4
Engine speed, rpm	4 000	4 000	4 000	4 000
Fuel flow, lb/hr	12.38	16.22	20.61	27.02
Air flow, lb/hr	490	460	500	600
Equivalence ratio	0.36	0.51	0.59	0.65
Turbo speed, rpm	32 050	39 800	47 340	59 020
Intercooled	No	No	No	Yes
Engine inlet pressure, atm	1.08	1.147	1.214	1.358
Turbine inlet pressure, atm	1.057	1.047	1.067	1.074
Engine inlet temperature, K	175.7	314.26	323.15	315.37
Turbine inlet temperature, K	669	830	903	925
Main injection start, deg BTC	48	46	48	55
Main injection end, deg BTC	25	18	16	16
Pilot injection start, deg BTC	54	61	66	70
Pilot injection end, deg BTC	34	32	38	42
Volumetric efficiency, percent	110.7	99.6	105.5	111.0
Brake horsepower, BHP, hp	17.64	31.49	41.00	52.70
Brake mean effective pressure, BMEP, psi (kPa)	43.3 (298)	76.8 (529)	100.4 (693)	129.0 (890)
Brake specific fuel consumption, BSFC, lb/bhp-hr	0.7018	0.5151	0.5026	0.5127

TABLE III. - RESULTS OF HEAT RELEASE ANALYSIS OF THE 1007R RIG ENGINE

[Expressed as percent of introduced fuel energy.]

Case number	Percent thermal efficiency plus percent change in sensible internal energy	Percent heat transfer to structure	Percent heat loss to crevice volume and leakage area
1	42	57	<1
2	46	53	↓
3	48	51	
4	44	55	

TABLE IV. - PREDICTED PERFORMANCE DATA FOR THE 1007R RIG ENGINE

	Case number			
	1	2	3	4
Volumetric efficiency, percent	108.4	115	125	142.5
Indicated power, hp	28.33	44.1	54.78	70.78
Indicated mean effective pressure, IMEP, psi (kPa)	88.2 (609.0)	135.9 (937)	163.8 (1160)	216.3 (1491)
Indicated specific fuel consumption, ISFC, lb/hp-hr (g/kW-hr)	0.3485 (212)	0.3617 (220)	0.3699 (225)	0.3896 (237)
Exhaust temperature, K	802	1272	1485	1671

TABLE V. - EFFECT OF COMBUSTION DURATION ON 1007R RIG ENGINE PERFORMANCE

[Engine speed, 4000 rpm; brake mean effective pressure, BMEP, 890 kPa.]

	Combustion duration, deg crankshaft angle				
	15.5	31.5	44.4	71.5	114.2
Indicated power, hp	70.81	70.73	70.78	66.91	64.82
Thermal efficiency, percent	34.6	34.5	34.6	32.7	31.6
Indicated specific fuel consumption, ISFC, lb/hp-hr (g/kW-hr)	0.3896 (237)	0.3896 (237)	0.3896 (237)	0.4126 (251)	0.4258 (259)
Indicated mean effective pressure, IMEP, psi (kPa)	216.3 (1491)	216.1 (1490)	216.3 (1491)	204.8 (1412)	197.8 (1364)
Exhaust temperature, K	1635	1645	1671	1732	1730

TABLE VI. - COMPARISON OF PERFORMANCE IMPROVEMENT

[Expressed as percent change in performance.]

	Spark timing[a]	Higher compression ratio[b]	Reduced leakage[c]	Intake/ exhaust pressure[d]
Indicated specific fuel consumption, ISFC	-1.7	-4.4	-15.7	3.8
Power	1.4	3.8	12.4	32
Exhaust temperature	-1.7	1.3	-----	16.8
Volumetric efficiency	0	0	-0.5	33
Indicated mean effective pressure, IMEP	1.4	3.7	12.8	31

[a]Increase in spark timing from 8° to 20° BTC.
[b]Increase in compression ratio from 7.5 to 8.92.
[c]Reduction in leakage area from 0.02 to 0 cm^2.
[d]Increase in intake pressure from 1.18 to 1.5 atm; exhaust pressure, 1.074 atm.

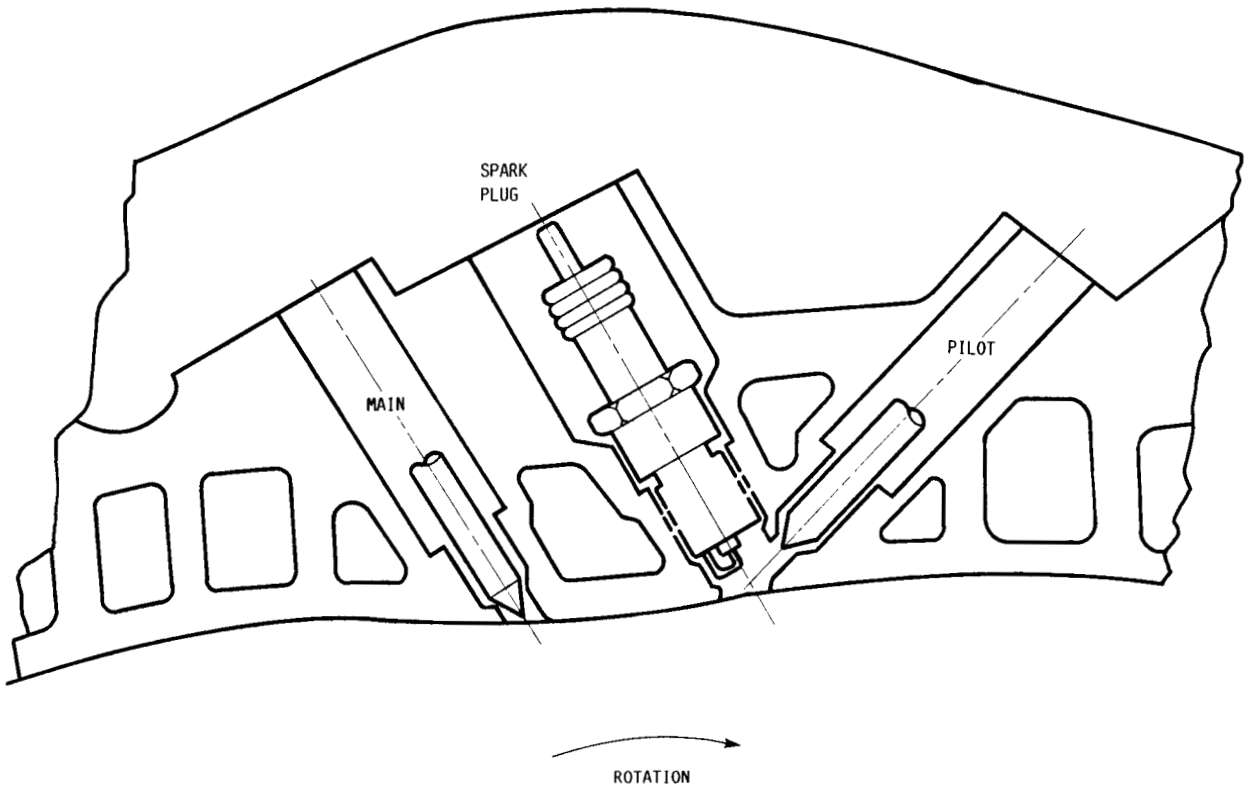

FIGURE 1. - CROSS SECTION OF COMBUSTION CHAMBER, SHOWING LOCATIONS OF PILOT AND MAIN FUEL INJECTORS AND IGNITER.

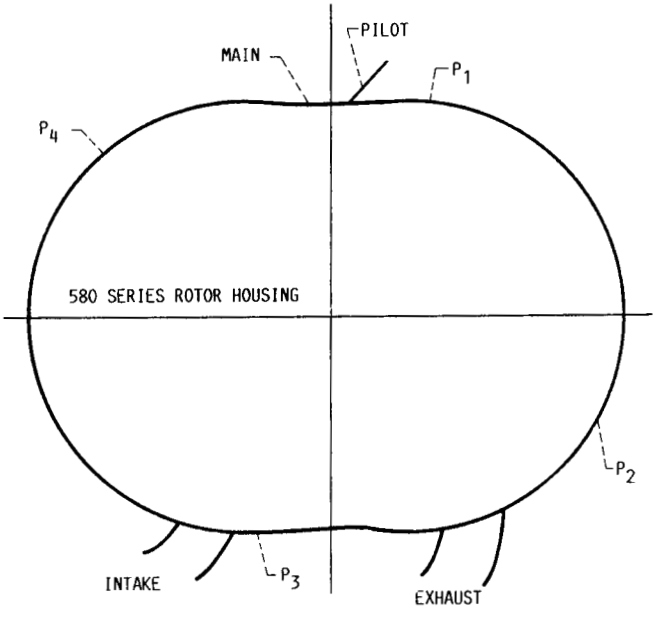

FIGURE 2. - POSITIONS OF PRESSURE TRANSDUCERS P IN 1007R ENGINE ROTOR HOUSING.

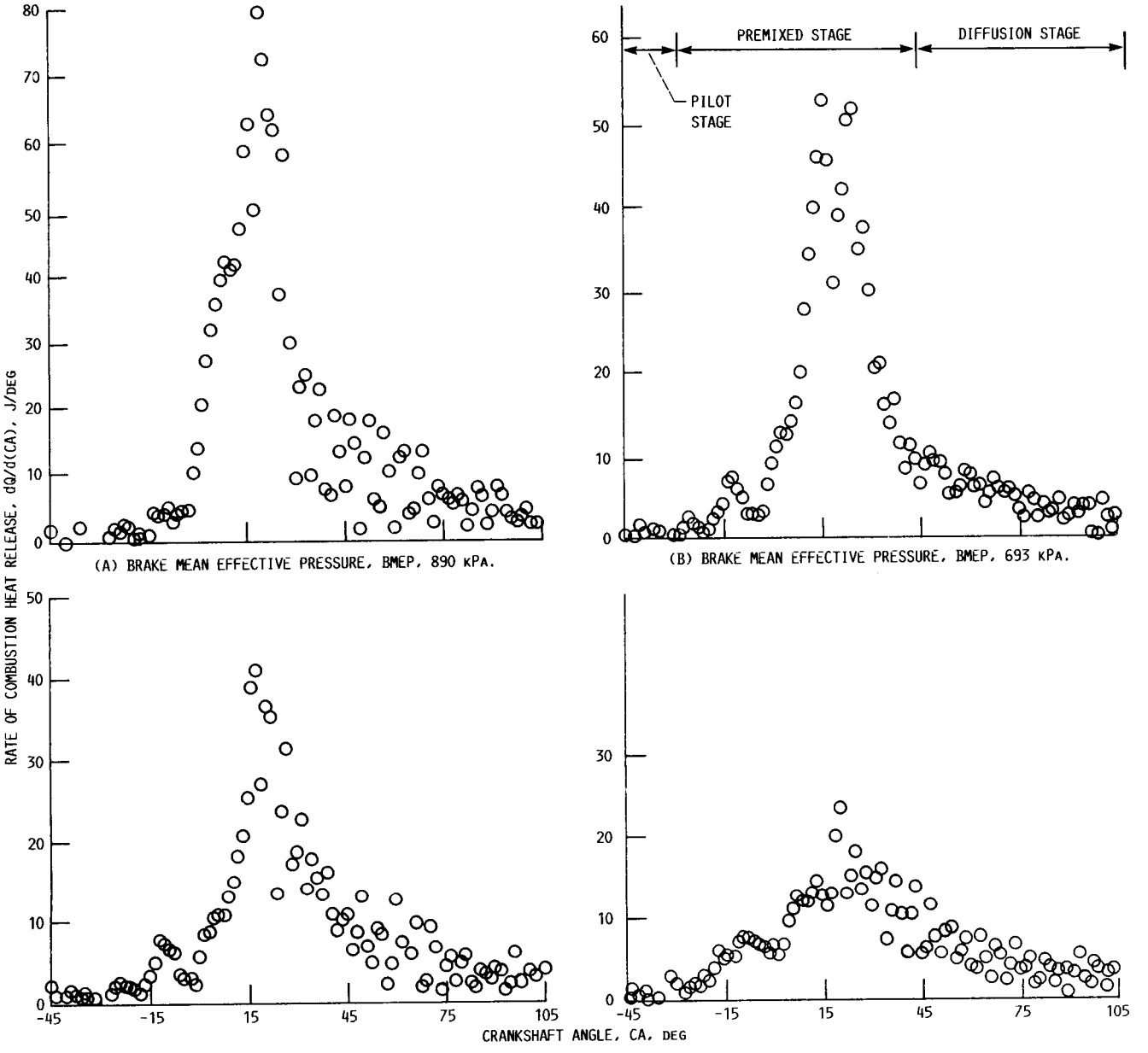

(A) BRAKE MEAN EFFECTIVE PRESSURE, BMEP, 890 kPa.

(B) BRAKE MEAN EFFECTIVE PRESSURE, BMEP, 693 kPa.

(C) BRAKE MEAN EFFECTIVE PRESSURE, BMEP, 529 kPa.

(D) BRAKE MEAN EFFECTIVE PRESSURE, BMEP, 298 kPa.

FIGURE 3. - HEAT RELEASE RATE. ENGINE SPEED, 4000 RPM.

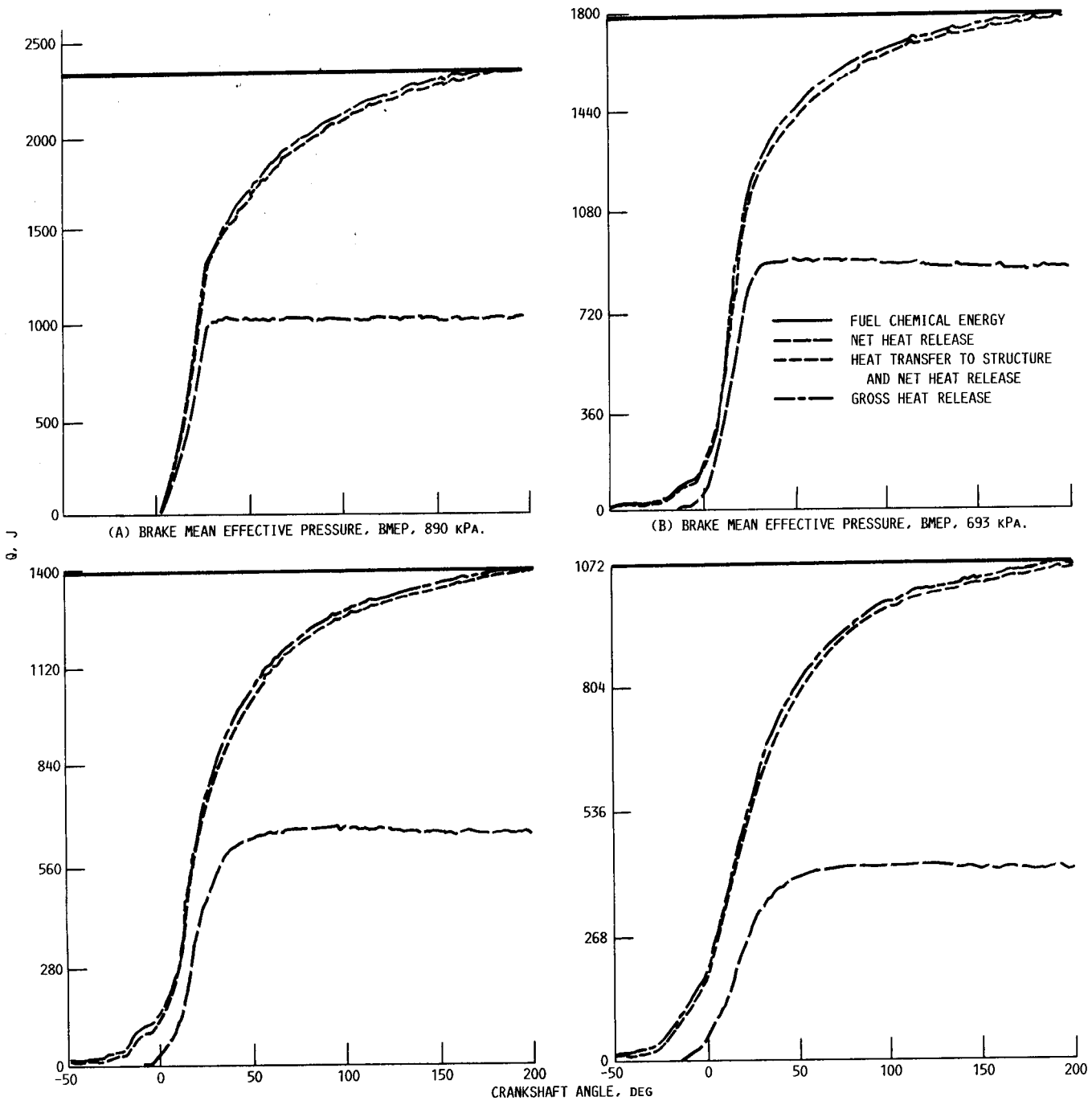

(A) BRAKE MEAN EFFECTIVE PRESSURE, BMEP, 890 kPa.

(B) BRAKE MEAN EFFECTIVE PRESSURE, BMEP, 693 kPa.

(C) BRAKE MEAN EFFECTIVE PRESSURE, BMEP, 529 kPa.

(D) BRAKE MEAN EFFECTIVE PRESSURE, BMEP, 298 kPa.

FIGURE 4. - INTEGRATED HEAT RELEASE. ENGINE SPEED, 4000 RPM.

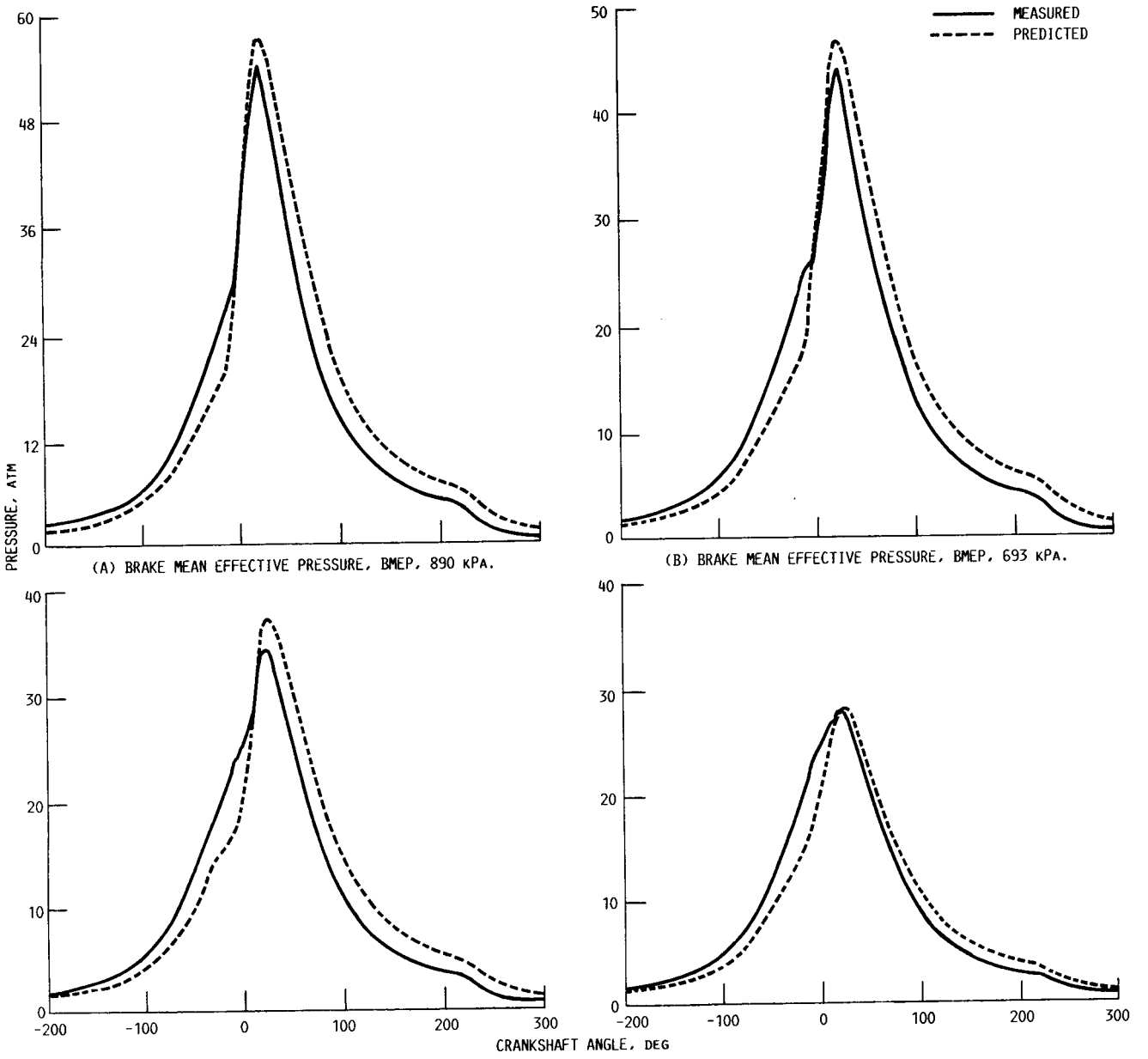

(A) BRAKE MEAN EFFECTIVE PRESSURE, BMEP, 890 kPa.

(B) BRAKE MEAN EFFECTIVE PRESSURE, BMEP, 693 kPa.

(C) BRAKE MEAN EFFECTIVE PRESSURE, BMEP, 529 kPa.

(D) BRAKE MEAN EFFECTIVE PRESSURE, BMEP, 298 kPa.

FIGURE 5. - COMPARISON OF MEASURED AND PREDICTED CHAMBER PRESSURES. ENGINE SPEED, 4000 RPM.

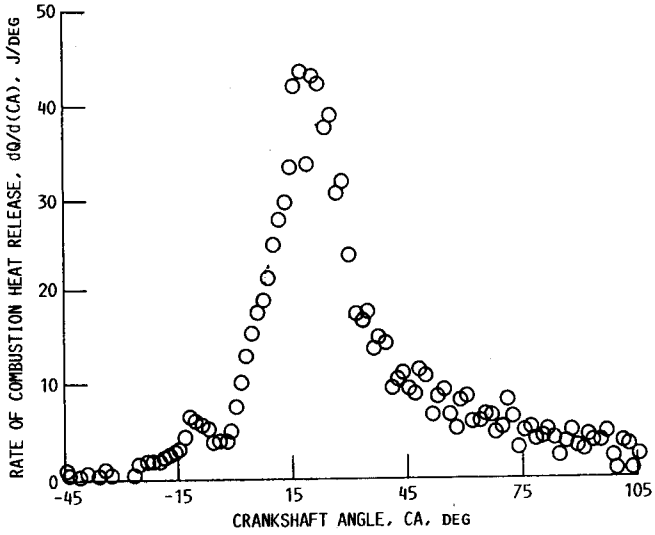

FIGURE 6. - AVERAGE HEAT RELEASE RATE. ENGINE SPEED, 4000 RPM.

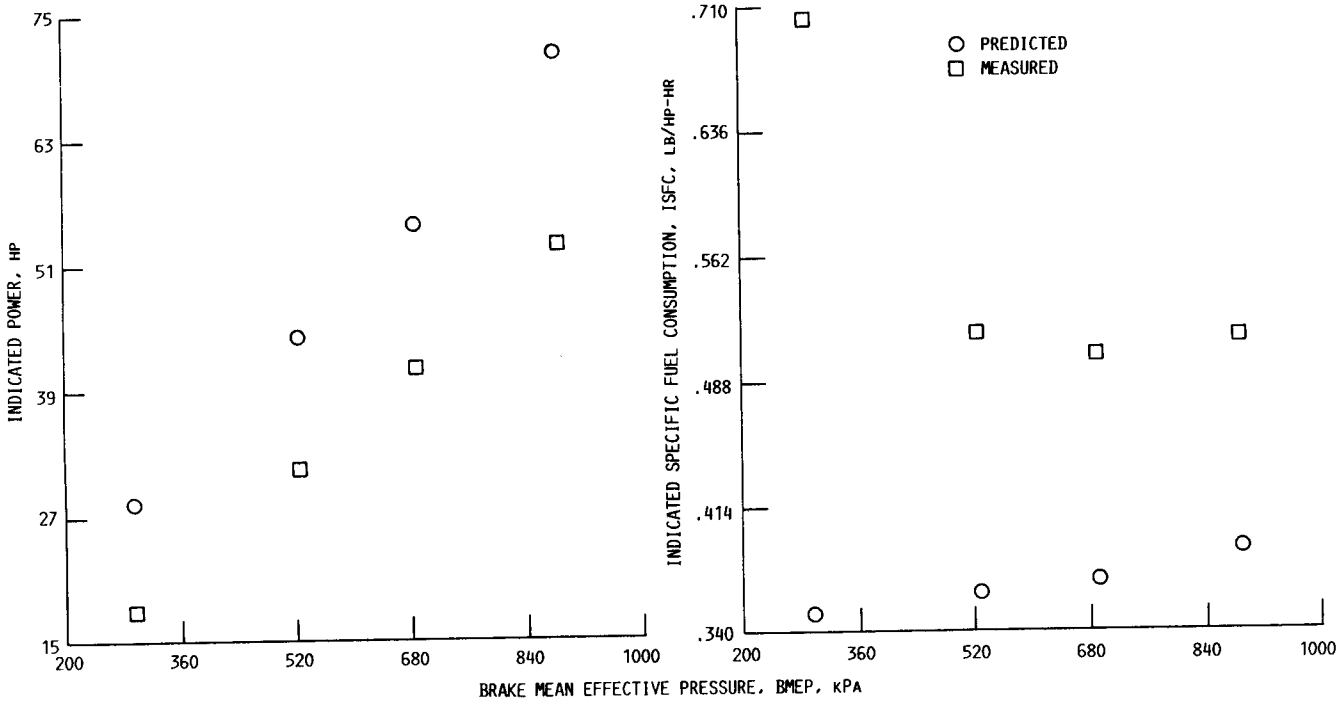

(A) COMPARISON OF INDICATED OUTPUT POWER VALUES PREDICTED BY THE SIMULATION WITH BRAKE HORSEPOWER AT FOUR LOADS AND 4000 RPM.

(B) COMPARISON OF INDICATED SPECIFIC FUEL CONSUMPTION VALUES PREDICTED BY THE SIMULATION WITH EXPERIMENTAL BRAKE SPECIFIC FUEL COMSUMPTION AT FOUR LOADS AND 4000 RPM.

FIGURE 7. - 1007R STRATIFIED-CHARGE ROTARY COMBUSTION ENGINE PERFORMANCE RESULTS.

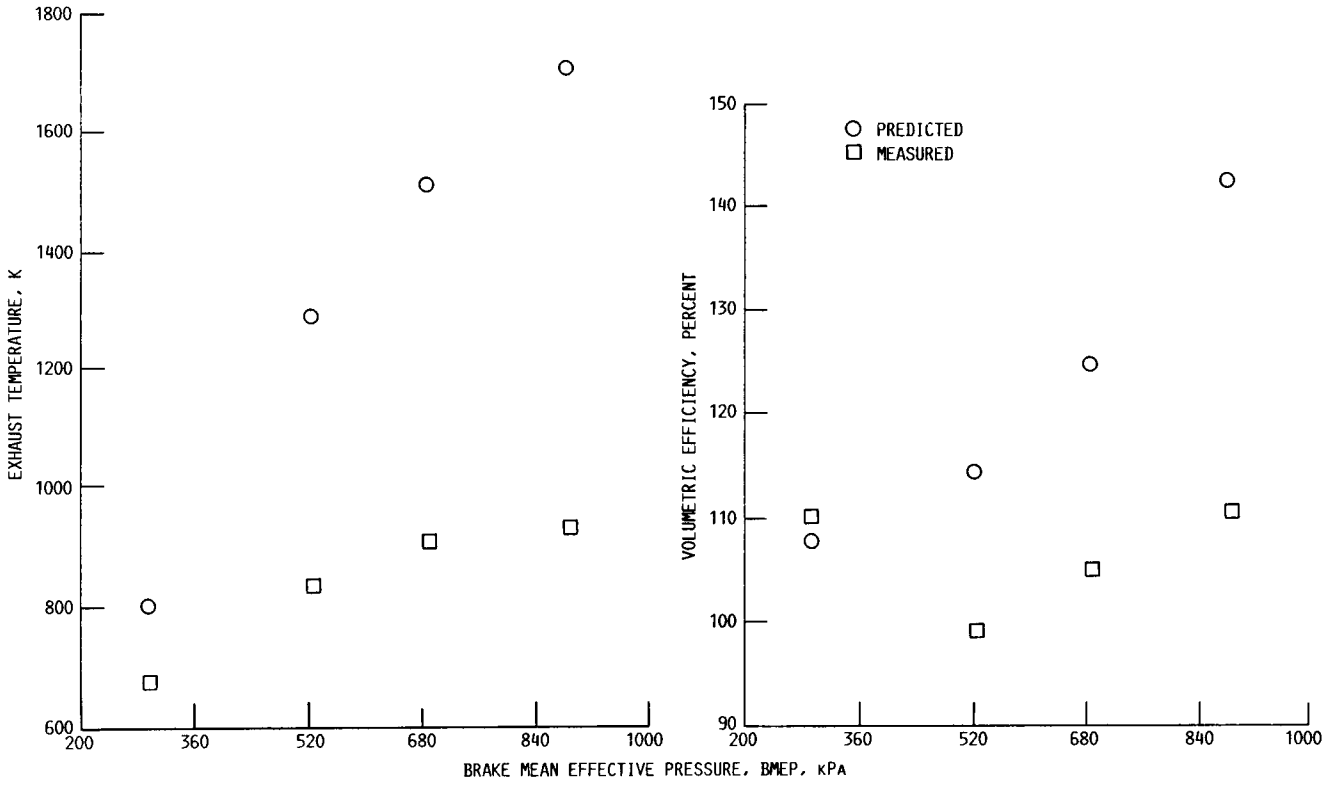

FIGURE 8. - COMPARISON OF PREDICTED AND MEASURED VOLUMETRIC EFFICIENCY AND EXHAUST TEMPERATURE.

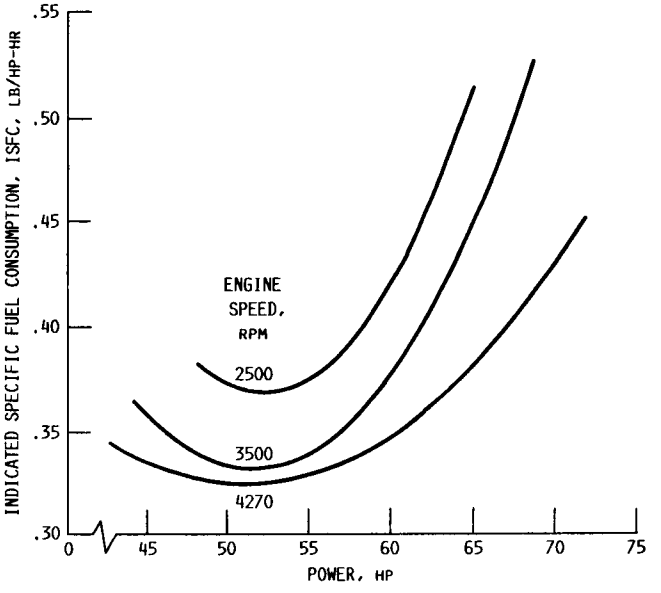

FIGURE 9. - PREDICTED 1007R RIG ENGINE PERFORMANCE AND FUEL CONSUMPTION.

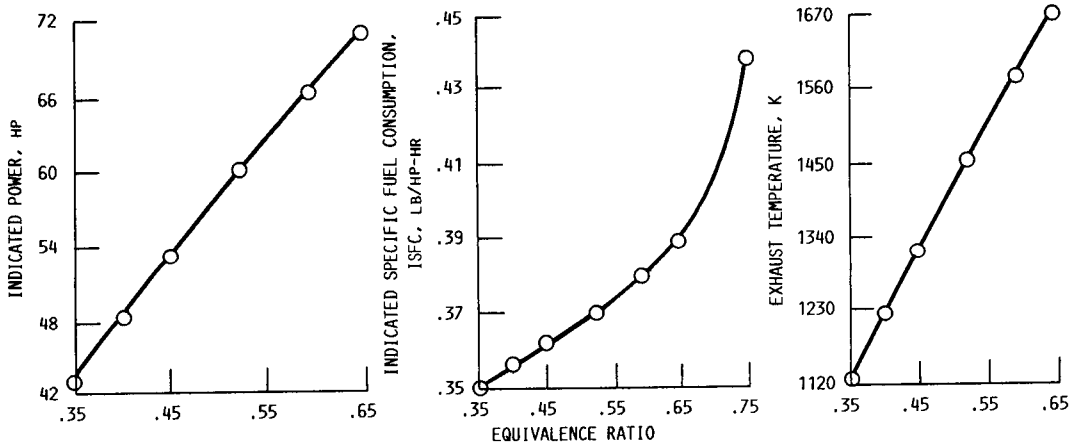

(A) INDICATED POWER OUTPUT.

(B) INDICATED SPECIFIC FUEL CONSUMPTION, ISFC.

(C) EXHAUST TEMPERATURE.

FIGURE 10. - VARIATION IN POWER OUTPUT, INDICATED SPECIFIC FUEL CONSUMPTION, AND EXHAUST TEMPERATURE WITH EQUIVALENCE RATIO. ENGINE SPEED, 4000 RPM.

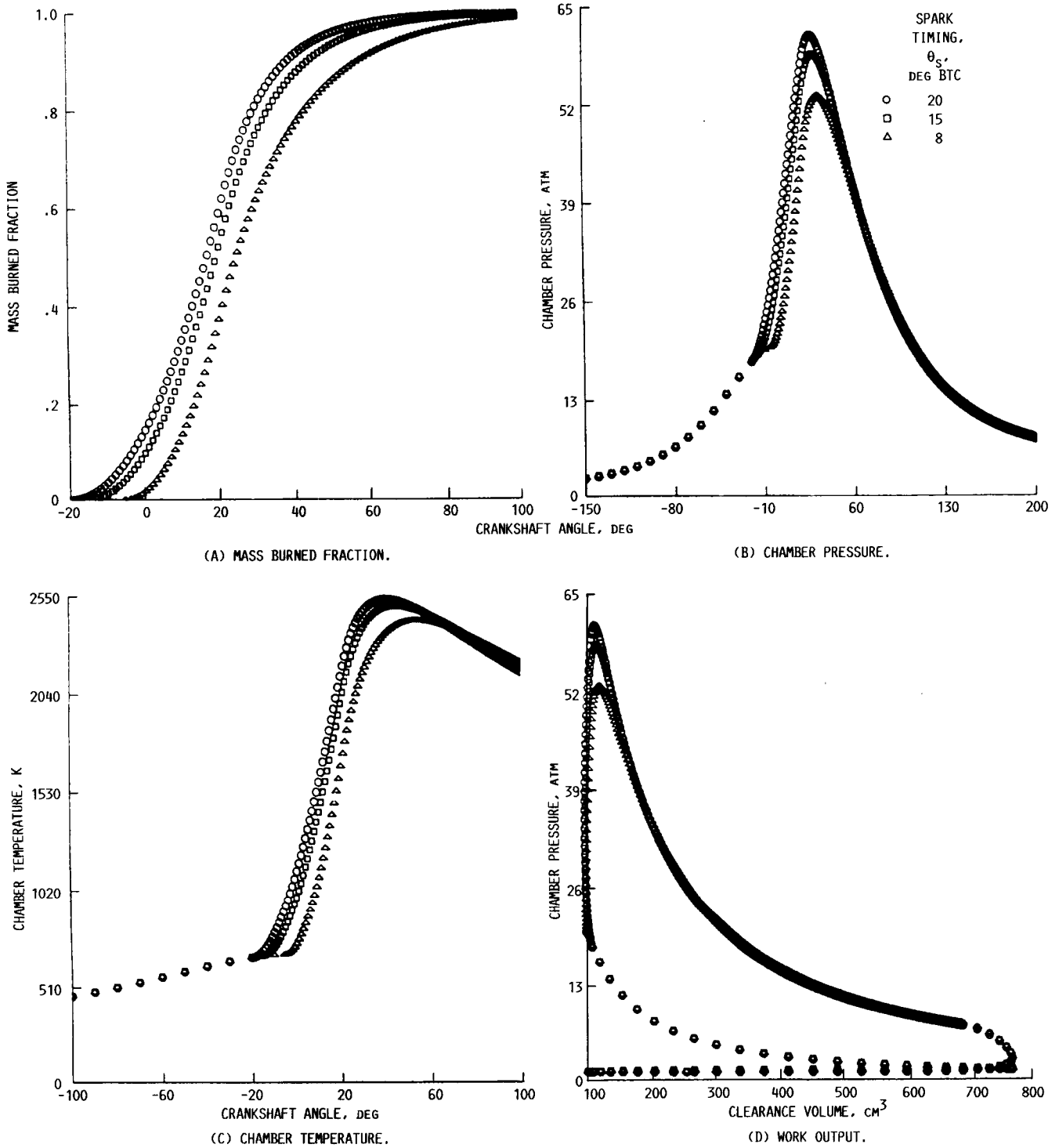

(A) MASS BURNED FRACTION.

(B) CHAMBER PRESSURE.

(C) CHAMBER TEMPERATURE.

(D) WORK OUTPUT.

FIGURE 11. - EFFECT OF SPARK TIMING ON MASS BURNED FRACTION, CHAMBER PRESSURE AND TEMPERATURE, AND POWER OUTPUT OF THE 1007R RIG. ENGINE SPEED, 4000 RPM; BRAKE MEAN EFFECTIVE PRESSURE, BMEP, 890 KPA.

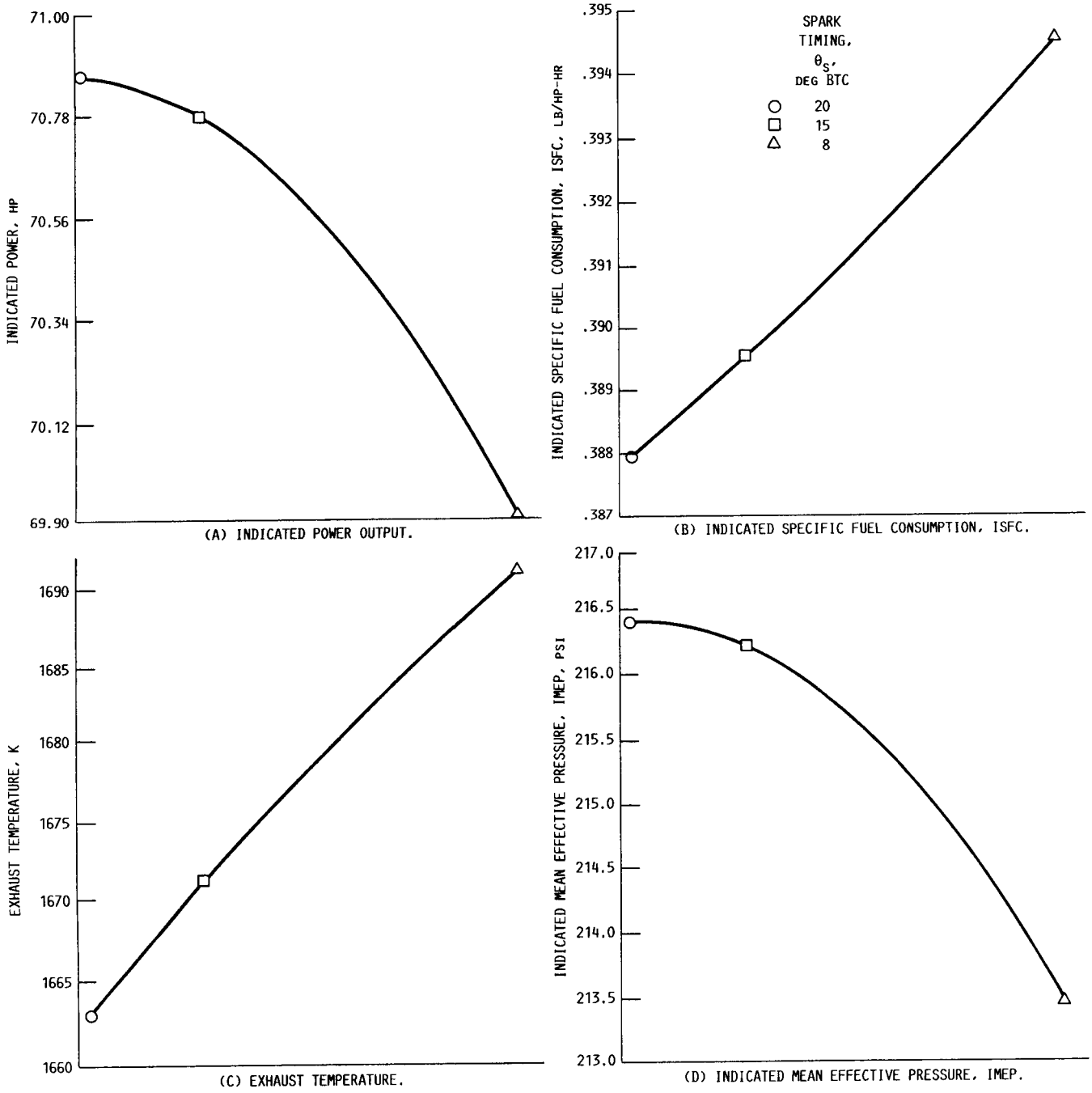

FIGURE 12. - EFFECT OF SPARK TIMING ON ENGINE PERFORMANCE. ENGINE SPEED, 4000 RPM; BRAKE MEAN EFFECTIVE PRESSURE, BMEP, 890 KPA.

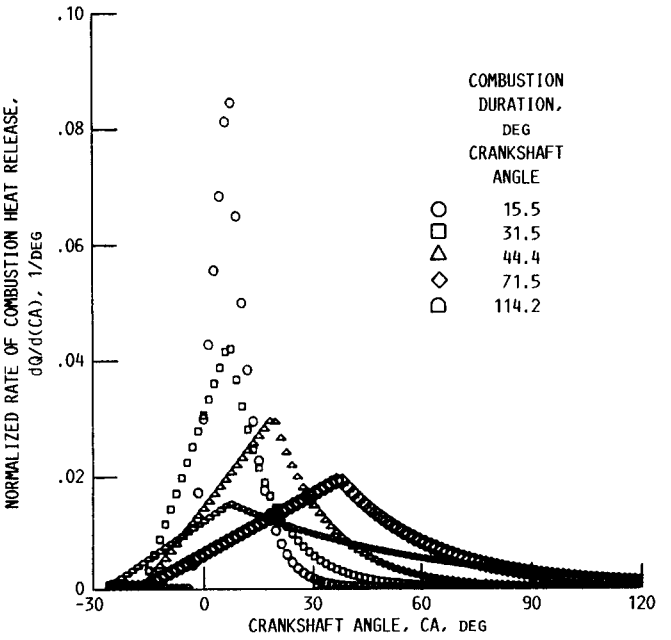

FIGURE 13. - EMPIRICAL HEAT RELEASE RATE MODELS USED TO STUDY EFFECT OF COMBUSTION DURATION ON ENGINE PERFORMANCE.

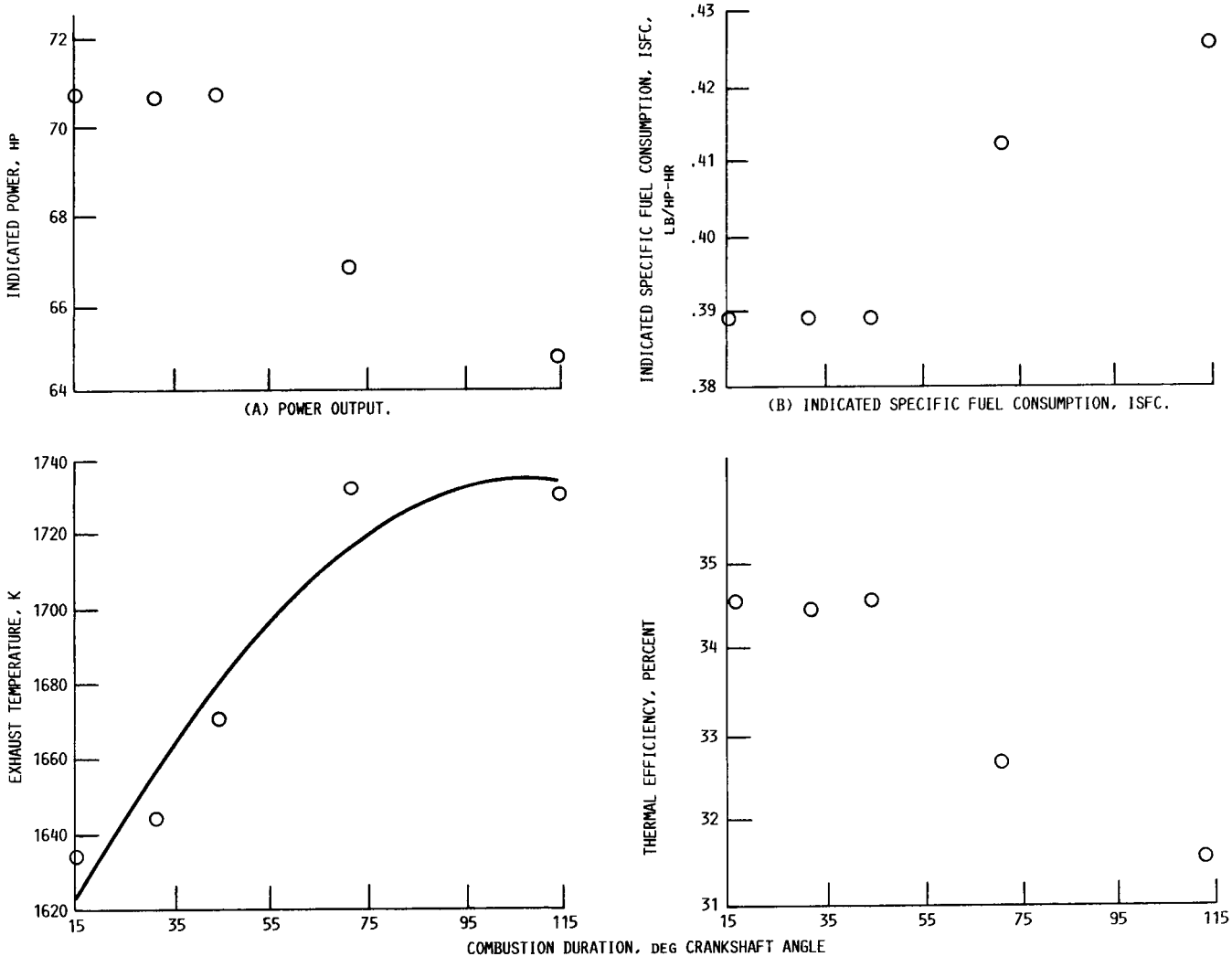

FIGURE 14. - EFFECT OF COMBUSTION DURATION ON ENGINE PERFORMANCE. ENGINE SPEED, 4000 RPM; BRAKE MEAN EFFECTIVE PRESSURE, BMEP, 890 KPA.

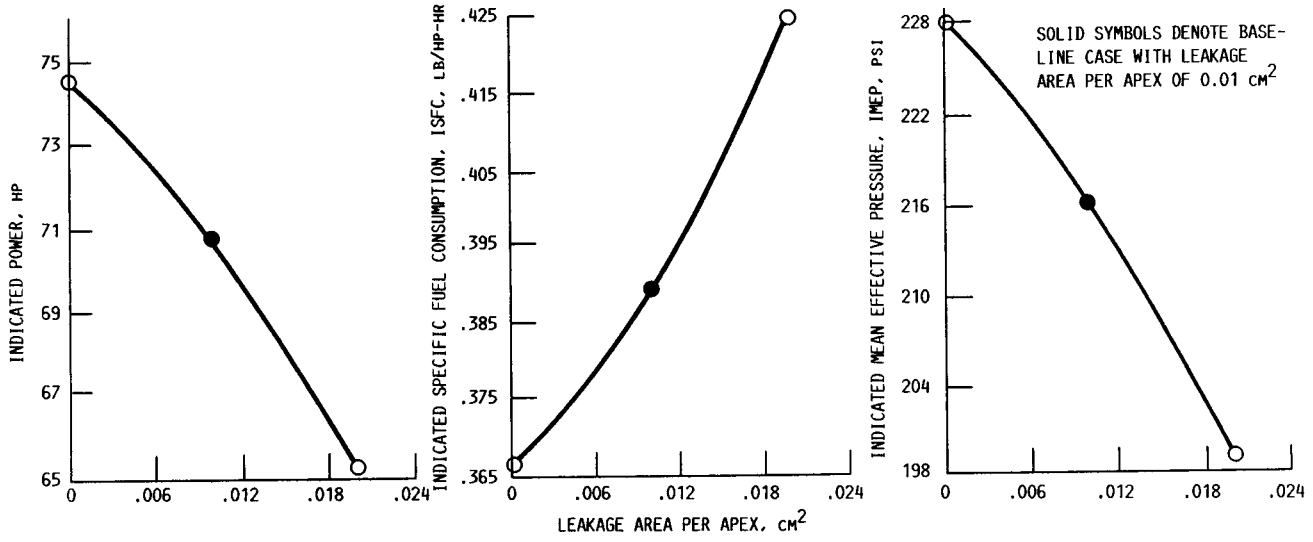

(A) INDICATED POWER OUTPUT.

(B) INDICATED SPECIFIC FUEL CONSUMPTION, ISFC.

(C) INDICATED MEAN EFFECTIVE PRESSURE, IMEP.

FIGURE 15. - EFFECT OF REDUCED LEAKAGE ON ENGINE PERFORMANCE. ENGINE SPEED, 4000 RPM; BRAKE MEAN EFFECTIVE PRESSURE, BMEP, 890 KPA.

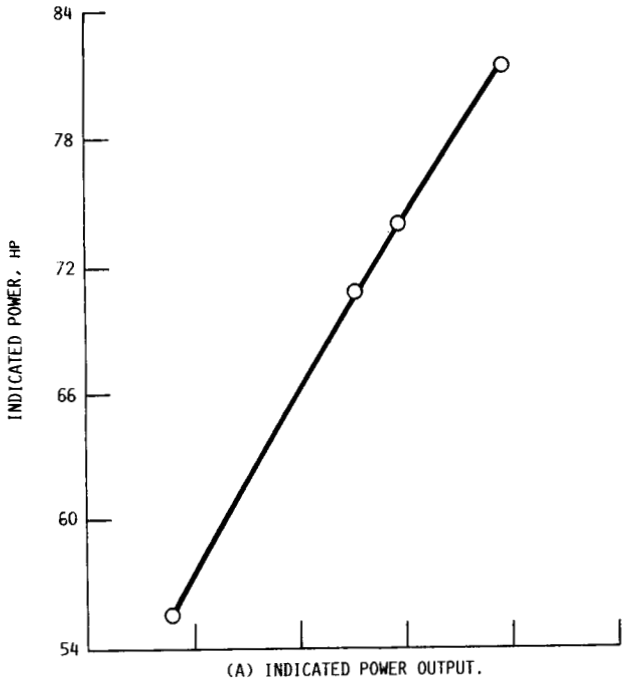

(A) INDICATED POWER OUTPUT.

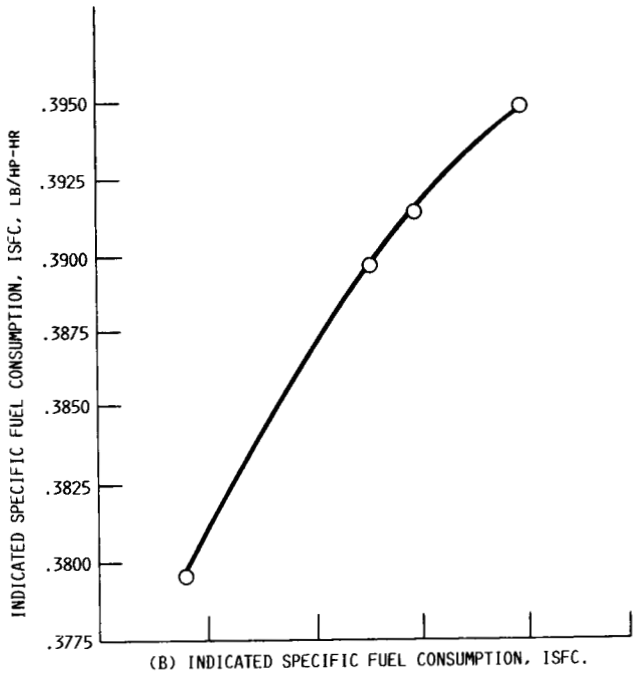

(B) INDICATED SPECIFIC FUEL CONSUMPTION, ISFC.

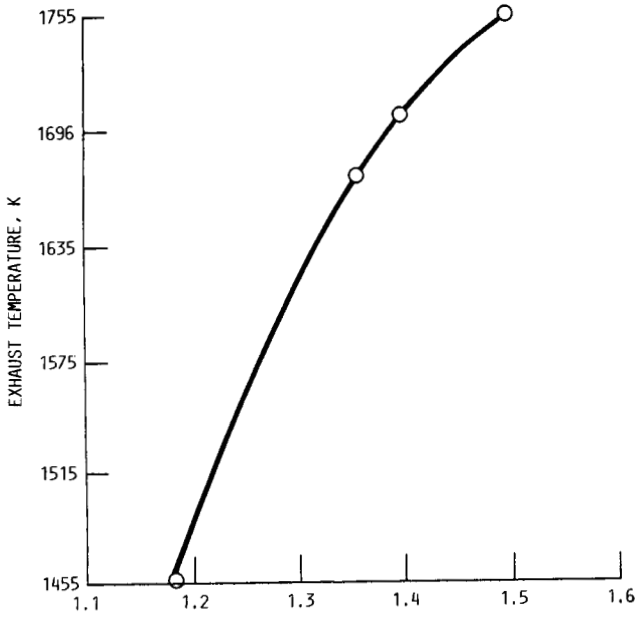

(C) EXHAUST TEMPERATURE.

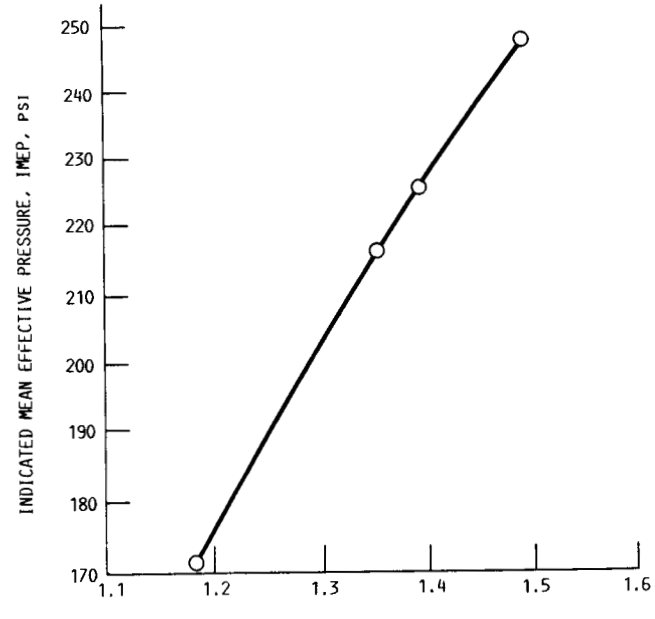

(D) INDICATED MEAN EFFECTIVE PRESSURE, IMEP.

INTAKE PRESSURE, ATM

FIGURE 16. - EFFECT OF INTAKE/EXHAUST PRESSURE RATIO. ENGINE SPEED, 4000 RPM; BRAKE MEAN EFFECTIVE PRESSURE, BMEP, 890 KPA; EXHAUST PRESSURE, 1.074 ATM.

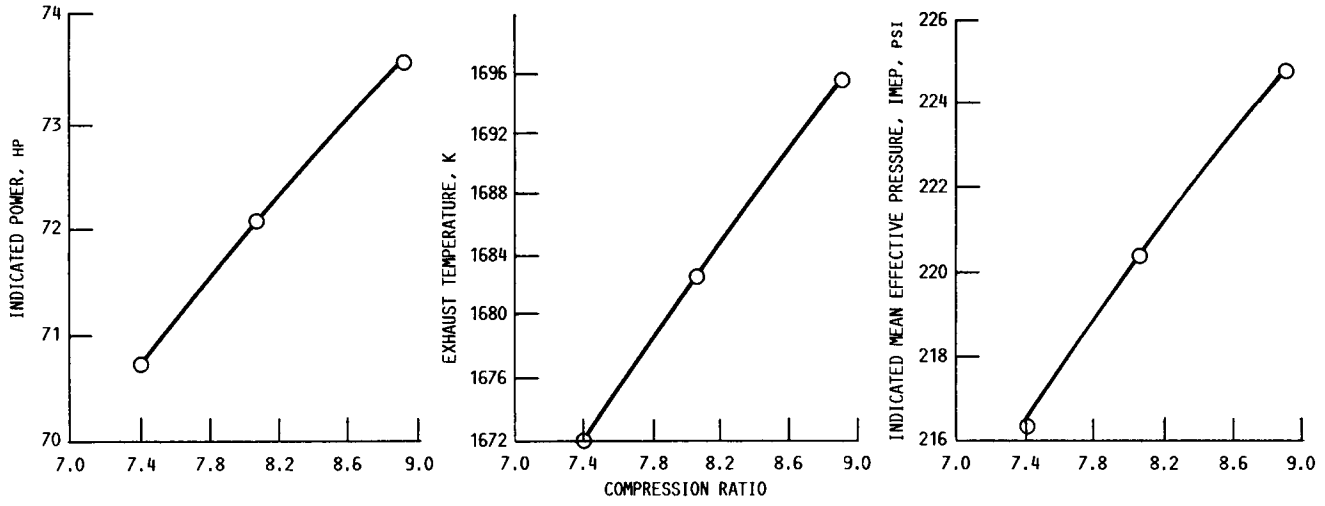

(A) INDICATED POWER OUTPUT.

(B) EXHAUST TEMPERATURE.

(C) INDICATED MEAN EFFECTIVE PRESSURE, IMEP.

FIGURE 17. - EFFECT OF COMPRESSION RATIO ON ENGINE PERFORMANCE. ENGINE SPEED, 4000 RPM; BRAKE MEAN EFFECTIVE PRESSURE, BMEP, 890 KPA.

NASA
National Aeronautics and Space Administration

Report Documentation Page

1. Report No.	2. Government Accession No.	3. Recipient's Catalog No.
NASA TM-100134		

4. Title and Subtitle	5. Report Date
Performance and Combustion Characteristics of Direct-Injection Stratified-Charge Rotary Engines	December 1987
	6. Performing Organization Code
7. Author(s)	8. Performing Organization Report No.
Hung Lee Nguyen	E-3684
	10. Work Unit No. 505-62-11
9. Performing Organization Name and Address	11. Contract or Grant No.
National Aeronautics and Space Administration Lewis Research Center Cleveland, Ohio 44135-3191	
	13. Type of Report and Period Covered
12. Sponsoring Agency Name and Address	Technical Memorandum
National Aeronautics and Space Administration Washington, D.C. 20546-0001	14. Sponsoring Agency Code

15. Supplementary Notes

16. Abstract

Computer simulations of the direct-injection stratified-charge (DISC) Wankel engine have been used to calculate heat release rates and performance and efficiency characteristics of the 1007R engine. Engine pressure data have been used in a heat release analysis to study the effects of heat transfer, leakage, and crevice flows. Predicted engine performance data are compared with experimental test data over a range of engine speeds and loads. An examination of methods to improve the performance of the Wankel engine with faster combustion, reduced leakage, higher compression ratio, and turbocharging is presented.

17. Key Words (Suggested by Author(s))	18. Distribution Statement
Direct-injection stratified-charge rotary engines; Heat release analysis; Combustion; Engine performance	Unclassified - Unlimited Subject Category 07

19. Security Classif. (of this report)	20. Security Classif. (of this page)	21. No of pages	22. Price*
Unclassified	Unclassified	28	A03

NASA FORM 1626 OCT 86

*For sale by the National Technical Information Service, Springfield, Virginia 22161